The multi PAM2 protein Upa2 functions as novel core component of endosomal mRNA transport

Silke Jankowski^{1, †}, Thomas Pohlmann^{1, †}, Sebastian Baumann^{1, #}, Kira Müntjes¹, ¹, Senthil Kumar Devan¹, Sabrina Zander¹ and Michael Feldbrügge^{1, *}

[†] equal contribution

¹ Heinrich Heine University Düsseldorf, Institute for Microbiology, Cluster of Excellence on Plant Sciences, 40204 Düsseldorf, Germany

present address: Cell and Developmental Biology, Centre for Genomic Regulation (CRG),Barcelona, Spain

Running title: Multi PAM2 protein for mRNA transport

Word count: 4275

Key words: endosome / microtubule / MLLE domain / PAM2 motif / poly(A)-binding protein / RNA transport

^{*} Corresponding author:

Dr. Michael Feldbrügge

Institute for Microbiology, Cluster of Excellence on Plant Sciences

Heinrich Heine University Düsseldorf; 40204 Düsseldorf, Germany,

Phone: +49 (211) 81-15475,

feldbrue@hhu.de

1 Abstract

2 mRNA transport determines spatiotemporal protein expression. Transport units are higher-3 order ribonucleoprotein complexes containing cargo mRNAs, RNA-binding proteins and 4 accessory proteins. Endosomal mRNA transport in fungal hyphae belongs to the best-studied 5 translocation mechanisms. Although several factors are known, additional core components 6 are missing. Here, we describe the 232 kDa protein Upa2 containing multiple PAM2 motifs 7 (poly[A]-binding protein [Pab1] associated motif 2) as a novel core component. Loss of Upa2 8 disturbs transport of cargo mRNAs and associated Pab1. Upa2 is present on almost all 9 transport endosomes in an mRNA dependent-manner. Surprisingly, all four PAM2 motifs are 10 dispensable for function during unipolar hyphal growth. Instead, Upa2 harbours a novel N-11 terminal effector domain as important functional determinant as well as a C-terminal GWW 12 motif for specific endosomal localisation. In essence, Upa2 meets all the criteria of a novel 13 core component of endosomal mRNA transport and appears to carry out crucial scaffolding 14 functions.

15

Jankowski, Pohlmann et al.

16 Introduction

17 Active transport of mRNAs determines when and where proteins are synthesised. Such trafficking events are important for a wide variety of different cellular processes like 18 19 asymmetric cell division, polar growth, embryonic development and neuronal activity [1, 2]. Several mRNA translocation mechanisms have been described. During cytokinesis of 20 21 Saccharomyces cerevisiae, for example, the actin-dependent transport of ASH1 mRNA is 22 mediated by the concerted binding of the RNA-binding proteins (RBP) She2p and She3p. 23 These RBPs connect the cargo mRNA to the myosin motor Myo4 for transport towards the 24 daughter cell [3, 4]. In highly polarised cells such as fungal hyphae and neurons, mRNAs are 25 transported along microtubules over long distances. Here, molecular motors such as kinesins and dynein are involved. Among the best studied examples of microtubule-dependent 26 27 translocation is the mRNA transport on shuttling endosomes during polar hyphal growth in 28 the fungus Ustilago maydis [5].

29 Upon infection of corn, U. maydis switches from budding to hyphal growth [6, 7]. The resulting infectious hyphae grow with a defined axis of polarity: they expand at the apical 30 31 pole and insert septa at the basal pole resulting in the formation of characteristic sections devoid of cytoplasm. In this growth mode, hyphae depend on active transport along 32 33 microtubules. Loss of long-distance transport results in aberrant hyphal growth. Characteristic 34 of this defect is the formation of bipolar growing cells. Important carriers are Rab5a-positive 35 endosomes that shuttle along microtubules by the concerted action of the plus-end directed Kinesin-3 type motor Kin3 and the minus-end directed cytoplasmic dynein Dyn1/2 [8, 9]. 36 37 These endosomes carry characteristic markers of early endosomes involved in endocytosis [10]. However, during polar growth they also function as transport endosomes moving 38 39 organelles, like peroxisomes, and mRNAs with associated ribosomes attached to their 40 cytoplasmic surface [11, 12].

Jankowski, Pohlmann et al.

41 The key RNA-binding protein for mRNA transport is Rrm4, an RRM (RNA recognition 42 motif) protein containing tandem N-terminal RRMs separated by a spacer from a third RRM domain (Fig 1A). The mRNAs of all four septins were identified to be important cargo 43 44 mRNAs, which are most likely translationally active while being transported on endosomes [12-14]. Consequently, the translation products Cdc3, Cdc10, Cdc11 and Cdc12 form 45 46 heteromeric complexes on the cytoplasmic surface of endosomes in an Rrm4-dependent 47 manner. These septin complexes are delivered to the hyphal growth pole to form a 48 longitudinal gradient of filaments [12, 14]. A recent transcriptome-wide view of endosomal 49 mRNA transport revealed that Rrm4 binds thousands of mRNAs preferentially in their 3' 50 UTR in close proximity to the small glycine rich protein Grp1. This extensive mRNA 51 transport is most likely needed for the distribution of mRNAs within the fast-growing hypha 52 as well as for the transport of specific mRNAs encoding e.g. septins for heterooligomerisation 53 [15].

54 At its C-terminus, Rrm4 carries two MademoiseLLE (MLLE) domains that function as 55 peptide binding pockets for specific interaction with the PAM2-like motifs of Upa1. Upa1 56 links Rrm4-containing mRNPs to transport endosomes using a FYVE zinc finger domain to recognise phosphatidylinositol-3-phosphate lipids of early endosomes. [16]. In addition, Upa1 57 also carries a classical PAM2 motif for interaction with the MLLE domain of the poly(A)-58 59 binding protein Pab1, an additional component of endosomal mRNPs [7, 17]. Although we already identified a number of components of endosomal mRNA transport, key factors might 60 still be missing. Here, we unravelled and characterized one such factor, the protein Upa2, a 61 62 second Ustilago PAM2 motif protein that had previously been identified by bioinformatic prediction of PAM2-containing proteins [16]. 63

64

Jankowski, Pohlmann et al.

65 **Results**

66 The PAM2-containing protein Upa2 interacts with Pab1

Upa2 (*Ustilago* PAM2 protein 2; UMAG_10350) is a 2121 amino acid (aa) protein with a
conserved coiled coil domain of unknown function at its C-terminus, as well as four PAM2
motifs for potential interaction with the MLLE domain of Pab1. One PAM2 motif is situated
at the immediate N-terminus and three in the central region of the protein (Fig 1A-B).

71 In order to validate the predicted PAM2 motifs we performed yeast two-hybrid studies 72 that have already been successfully applied to demonstrate an interaction between Pab1 and 73 the PAM2 motif of Upa1 [16]. Full-length Upa2 shows weak interaction with Pab1 but did 74 not interact with Upa1 or Rrm4 (Fig 1C, Fig EV1A-B). The latter is consistent with the 75 observation that PAM2-like motifs for Rrm4 interaction are missing in Upa2 [16]. Upon 76 mapping the interaction domain of Upa2 with Pab1 we observed that the PAM2-containing 77 N-terminal part of Upa2 (aa 1-1216) but not the C-terminal part (aa 1217-2121) interacted 78 with Pab1 (Fig 1C). The interaction of Upa2 with Pab1 was mediated by the MLLE domain 79 of Pab1, since this domain was necessary and sufficient for reporter gene expression in the 80 yeast two-hybrid system (Fig 1C, Fig EV1A). Mutational analysis of the PAM2 motifs in 81 Upa2 revealed that a single PAM2 motif was sufficient for interaction with the MLLE domain 82 of Pab1 or full length Pab1 (Fig EV1A). Mutating all PAM2 motifs resulted in loss of 83 interaction of Upa2 with the MLLE domain of Pab1 (Fig 1C) and strongly reduced interaction with Upa2 and full length Pab1 (Fig EV1A). 84

To verify this binding behaviour, we tested the interaction of the central PAM2 triplet of Upa2 (aa 834-1216) with the MLLE domains of Pab1 by GST-pulldown experiments using variants expressed in *Escherichia coli*. These experiments confirmed the specific interaction of the PAM2 motifs of Upa2 with the MLLE domain of Pab1. The interaction strength was

Jankowski, Pohlmann et al.

dependent on the number of functional PAM2 motifs (Fig 1D). As expected, PAM2 motifs of
Upa2 did not interact with Rrm4 (Fig EV1C-D).

Since coiled coil domains have been described as dimerization regions, we tested this in a yeast two-hybrid assay. When appended to both BD and AD reporter proteins the predicted C-terminal coiled coil domain of Upa2 supported yeast growth on selective medium suggesting that this region indeed functions as a dimerization domain (Fig 1E). Taken together, Upa2 contains multiple functional PAM2 motifs for interaction with Pab1 and a Cterminal dimerization domain. The interaction with Pab1 is the first hint that Upa2 might function in endosomal mRNA transport.

98 Upa2 is essential for efficient unipolar hyphal growth

99 If Upa2 is indeed important for endosomal mRNA transport, loss of Upa2 should exhibit 100 phenotypes similar to mutations in the previously identified transport components Rrm4 and 101 Upa1 [16]. To test this assumption, we generated upa2 deletion mutants in the genetic 102 background of laboratory strain AB33. In this strain, hyphal growth can be elicited 103 synchronously and reproducibly by switching the nitrogen source in the medium [18]. Hyphae 104 grow with a defined axis of polarity: they expand at the apical tip and insert septa at their base 105 leading to the formation of characteristic empty sections (Fig 2A). While loss of Upa2 did not 106 affect growth or alter shape of yeast cells (Fig EV2A-B) $upa2\Delta$ strains exhibited a bipolar 107 growth phenotype and the formation of empty sections was delayed. This aberrant growth 108 mode is typical for defects in microtubule-dependent transport and has been described for loss 109 of the key proteins of endosomal mRNA transport like Rrm4 and Upa1 (Fig 2A-B). 110 Analysing the $upa1\Delta/upa2\Delta$ double mutant revealed that the number of hyphae exhibiting 111 aberrant bipolar hyphal growth was not additive (Fig EV2C), providing genetic evidence that 112 both PAM2-containing proteins function in the same cellular process.

Jankowski, Pohlmann et al.

A second read-out for defects in the endosomal mRNA transport machinery is the unconventional secretion of chitinase Cts1 [16, 19]. Loss of Upa2 resulted in reduced extracellular Cts1 activity specifically during hyphal growth. This is reminiscent of defective Cts1 secretion upon deletion of *rrm4* and *upa1* (Fig EV2D). Hence, Upa2 might function in concert with Rrm4 and Upa1 during endosomal mRNA transport.

118 This hypothesis was supported by a phylogenetic analysis showing that orthologs of 119 Upa2 were found in several basidiomycete fungi with comparable spacing of the predicted 120 PAM2 motifs (Fig 2C). Consistent with the notion that Rrm4, Upa1 and Upa2 function 121 together, these fungi also had orthologs for Rrm4 and Upa1. Notably, Upa2 was absent in 122 Malassezia globosa, which presumably has lost the endosomal mRNA transport machinery, because it lacks a clear ortholog of Rrm4 (Fig 2C) [20]. In essence, the evolutionarily 123 124 conserved Upa2 is a novel factor essential for efficient unipolar growth that might function in 125 endosomal mRNA transport.

126 Upa2 shuttles on Rrm4-positive transport endosomes

127 upa2 and rrm4 appear to be genetically and phylogenetically linked. We therefore examined 128 whether the protein can also be found on transport endosomes by expressing a functional 129 version of Upa2 with C-terminally fused Gfp (eGfp, Clontech; Fig 2A-B; Fig EV2D). 130 Fluorescence microscopy revealed that in hyphae Upa2-Gfp localised exclusively in 131 bidirectionally moving units (Fig 3A, Video EV1). Movement was inhibited by benomyl 132 indicating that it was microtubule-dependent (Fig 3A, Video EV1). Importantly, Upa2-Gfp 133 shuttling resembled the movement of Rrm4-Gfp and Pab1-Gfp (Fig 3A, Video EV1). This 134 holds true for the amount of processive signals as well as for their velocity (Fig 3B-C). Hence, 135 Upa2 appeared to shuttle on Rrm4-positive transport endosomes [8, 16].

For experimental verification of endosomal shuttling we stained processive endosomeswith the lipophilic dye FM4-64 [10]. Using dual-colour dynamic live imaging, we detected

Jankowski, Pohlmann et al.

138 extensive co-localisation of Upa2-Gfp and FM4-64-stained, processively moving endosomes 139 (Fig 3D-E). Furthermore, we tested strains co-expressing Upa2-Gfp and Rrm4-mCherry or 140 Pab1-mCherry (functional C-terminal fusions with the monomeric red fluorescent protein 141 mCherry) [12, 13]. In this instant we also observed extensive co-localisation of Upa2 and 142 Rrm4 (Fig 3D-E, Video EV2) indicating that Upa2 was present on almost all shuttling 143 endosomes [8, 16]. Upa2-Gfp also co-localised with processively moving Pab1-mCherry (Fig 144 3D-E). However, unlike Rrm4, Pab1-mCherry additionally localised in the cytoplasm 145 resulting in diffuse and static signals that are easily detectable around the region of the 146 nucleus (Fig 3A, D) [12, 13]. Notably, Upa2 did not exhibit this cytoplasmic staining 147 indicating that it is not present in cytoplasmic Pab1-containing complexes, but specifically interacts with endosome-associated Pab1 (Fig 3A, D, E). In essence, Upa2 shuttles 148 149 exclusively on almost all Rrm4-positive transport endosomes supporting the notion that it is a 150 new component of endosomal mRNPs.

151 Endosomal localisation of Upa2 depends on the RNA-binding capacity of Rrm4

152 Since Upa2 proved to be an endosomal protein, we investigated the functional relationship 153 between Upa2 and Rrm4 by studying the subcellular localisation of endosomal mRNP 154 components in $rrm4\Delta$ strains. As previously described, the endosomal localisation of Upa1-155 Gfp is not affected in $rrm4\Delta$ strains, because its interaction is mRNA-independent and 156 mediated by its FYVE domain (Fig 4A-B, Video EV3) [16]. In contrast, Pab1-Gfp is no longer detectable on shuttling endosomes in $rrm4\Delta$ strains indicating that without Rrm4 no 157 158 mRNAs are transported on endosomes (Fig 4A-B, Video EV4) [13]. Interestingly, the 159 endosomal localisation of Upa2 was also no longer detectable in $rrm4\Delta$ strains (Fig 4A-B, 160 Video EV5) suggesting that the association of Upa2 depends on direct interaction with 161 endosomal mRNP components. In corresponding Western blot experiments, we verified that

Jankowski, Pohlmann et al.

loss of Rrm4 did not alter the protein amounts of Upa2-Gfp, Pab1-Gfp or Upa1-Gfp (FigEV2E).

164 To investigate a possible mRNA-dependent interaction of Upa2 with shuttling endosomes we studied the effect of the allele Rrm4^{mR1}-Rfp (Rrm4 variant with C-terminally fused 165 monomeric Rfp). Previously, it was shown that Rrm4^{mR1} carrying a loss of function mutation 166 167 in the first RRM domain resulted in drastically reduced RNA binding of Rrm4 [17]. Notably, Upa2 is no longer detectable on endosomes in a Rrm4^{mR1}-Rfp background, whereas for Pab1 168 169 we observed a strong reduction in movement (Fig 4C-D, Videos EV6-EV7). This indicates 170 that the recruitment of Upa2 to motile transport endosomes is dependent on the RNA-binding 171 capacity of Rrm4. Taken together, although loss of the endosomal components Upa1 and Upa2 results in similar defects during hyphal growth, the mode of endosomal localisation is 172 173 clearly different. Contrary to Upa1, endosomal localisation of Upa2 is mRNA-dependent, 174 suggesting an interaction with mRNA either directly or indirectly through a protein 175 component of mRNPs such as Pab1 that Upa2 binds via its PAM2 motifs.

Upa2 carries two functionally important regions, a N-terminal effector domain and a C terminal GWW motif

178 Since the mRNA-dependent localisation could be explained by the direct PAM2-dependent 179 interaction with Pab1, we tested the role of the identified PAM2 motifs of Upa2 with regards 180 to function and endosomal localisation. Therefore, we expressed Upa2-Gfp variants in 181 laboratory strain AB33 carrying mutations in one, in multiple and in all identified PAM2 182 motifs. Surprisingly, none of the PAM2 mutations affected the hyphal growth of U. maydis 183 indicating that the interaction of Upa2 with Pab1 is not essential for its role during hyphal 184 growth (Fig 5A-B). Furthermore, endosomal shuttling was not affected by mutating all four 185 PAM2s indicating that the interaction with Pab1 is dispensable for endosomal localisation 186 (Fig EV3A). Hence, Upa2 must contain so far unknown domains critical for endosomal 187 transport functions.

Jankowski, Pohlmann et al.

188 To map these domains, we studied N-terminal truncations carrying C-terminal Gfp 189 fusions (Fig 5C). Respective alleles were integrated at the homologous locus replacing the 190 endogenous copy of *upa2*. Expression was driven by the native *upa2* promoter. Removal of 191 the first 338 amino acids did not interfere with the function of the protein (Upa2-339-2121; 192 Fig 5C-D). However, additional truncations resulted in increase of bipolar hyphae indicating 193 reduced (Upa2-399-2121) or loss of function (Upa2-599-2121, 960-2121, 1217-2121, 1721-194 2121 and 1958-2121; Fig 5C-D, Fig EV3B). Importantly, protein amounts (e.g. 399-2121 and 195 399-2121; Fig EV3C) and endosomal shuttling of these versions were not drastically affected 196 (Fig 5E-F; Fig EV3D-E). Hence, a currently unknown effector domain important for 197 endosomal mRNA transport is located between amino acid position 339 and 599. Notably, the 198 non-functional variant Upa2-599-2121 still contained three PAM2 motifs, consistent with the 199 finding that the interaction with Pab1 is not sufficient for function.

200 For mapping of the domain that mediates endosomal localisation of Upa2, we assayed 201 additional N-terminal truncations. All variants still shuttled indicating that the last 163 amino 202 acids were sufficient for endosomal shuttling (Fig 5C, E-F). Upa2-1217-2121 did no longer 203 contain any PAM2 region for interaction with Pab1 (Fig 5C). This was consistent with the 204 finding that the PAM2 motifs of Upa2 were not essential for endosomal localisation. Closer 205 inspection by sequence comparison revealed a conserved GWW sequence at the very C-206 terminus (Fig 5G), which was shown in other proteins to function in protein/protein 207 interaction [21, 22]. Mutating this short sequence resulted in loss of shuttling without drastic 208 changes in protein amounts (Fig 5F, Fig EV3F). This holds true when testing the mutation in 209 the context of the full length protein (Fig 5H, Video EV8). Importantly, we also observed a 210 loss of function phenotype for this mutation, i.e. an increased number of bipolar hyphae (Fig 211 5H, Fig EV3G). This was not due to altered protein amounts (Fig EV3F). Thus, the conserved 212 C-terminal GWW motif is essential for endosomal localisation of Upa2 and endosomal 213 localisation is important for the function of the protein. In essence, besides the PAM2 motifs,

Jankowski, Pohlmann et al.

214 Upa2 contains a functionally important N-terminal effector domain and a C-terminal GWW

215 motif for interaction with an endosomal mRNP component (see Discussion).

216 Loss of Upa2 causes defects in the formation of endosomal mRNPs

217 Finally, we studied the role of Upa2 during endosomal transport in closer detail. Observation 218 of endosomal shuttling of Rrm4-Gfp, Upa1-Gfp and Rab5a-Gfp revealed that loss of Upa2 219 did not cause drastic alterations in bidirectional movement. We did notice a slight increase in 220 the velocity and amount of shuttling signals (Fig 6A-C, Videos EV9-EV12). In case of Rrm4-221 Gfp we observed that a substantial fraction of the protein also stained structures that 222 resembled microtubule bundles (Fig 6A; Fig EV4B). Consistently, in benomyl treated hyphae 223 bundle-like Rrm4-Gfp signals were no longer detected (Fig EV4B-C). This suggests that 224 Rrm4 localisation is disturbed in the absence of Upa2.

225 Interestingly, studying shuttling of Pab1-Gfp revealed that the amount of Pab1-positive 226 endosomes was reduced to about 50% (Fig. 6A-B), suggesting that Upa2 is needed for an 227 efficient interaction of Pab1-containing mRNAs with endosomes. To address this notion more 228 directly we applied RNA live imaging [23]. We studied four different target mRNAs of 229 Rrm4-dependent endosomal mRNA transport encoding the ubiquitin fusion protein Ubi1, the 230 small G protein Rho3, as well as the septins Cdc3 and Cdc12 (Fig EV4D) [12-14]. 231 Importantly, in the absence of Upa2 we observed in all four cases that the number of 232 processively transported mRNAs was reduced to about 50% (Fig 6D-E). This is consistent 233 with the shuttling of Pab1-Gfp that was reduced to comparable extend (Fig 6A-B). The range 234 of movement (Fig 6F) and the velocity (Fig EV4E) of transported *ubi1*, *rho3*, *cdc3* and *cdc12* 235 mRNA particles was not changed significantly. Thus, loss of Upa2 affects most likely 236 assembly or long-term association of mRNPs for transport.

An important function of endosomal septin mRNA transport is the local assembly of septin heteromeric subunits that are transported to hyphal growth poles to form higher-order

Jankowski, Pohlmann et al.

239 filaments with a gradient emanating from this pole [12, 14]. To address the role of Upa2 we 240 used a functional septin fusion protein Cdc3-Gfp as read-out (Cdc3 carrying eGfp at its N-241 terminus; notably the 5' and 3' untranslated regions of *cdc3* were preserved to keep potential 242 regulatory elements and Rrm4 binding sites intact) [12, 14]. Loss of Upa2 abolished 243 endosomal shuttling of Cdc3-Gfp and as an expected consequence also the Cdc3-Gfp 244 containing gradient at hyphal tips was no longer detectable (Fig 6G-I, Video EV14). The 245 strong reduction of septin protein on the surface of endosomes is consistent with the fact that 246 stable endosomal localisation of septin subunits depend on each other[14]. Since cdc3 and 247 cdc12 mRNAs are both reduced to 50% the amount of translated protein appears to be 248 insufficient to support endosomal localisation (see Discussion). In essence, Upa2 is essential 249 for the correct association of mRNAs, Pab1, as well as Rrm4, on endosomes. Thus, we 250 identified an endosome-specific and functionally important factor that functions as novel core 251 component of endosomal mRNA transport.

252

253 **Discussion**

254 Functional units of mRNA transport are higher-order mRNPs consisting of cargo mRNAs, 255 RNA-binding proteins and additional interacting proteins [5]. A crucial task is to differentiate 256 between core components that are essential to orchestrate transport, and accessory 257 components. The latter might mediate for example translational regulation of cargo mRNAs. 258 Here, we identified Upa2 as a novel core component of endosomal mRNA transport. This 259 interactor of the poly(A)-binding protein appears to be important for assembly or stabilisation 260 of higher-order mRNPs for endosomal transport suggesting that it functions as a scaffold 261 protein (Fig 7).

12

Jankowski, Pohlmann et al.

262 A novel multi PAM2 protein for endosomal mRNA transport

Upa2 is a large protein of 232 kDa that contains four functional PAM2 motifs for interaction
with the C-terminal MLLE domain of Pab1. It is known from earlier structural studies that the
C-terminal MLLE domain of human PABC1 forms a defined peptide pocket to accommodate
various PAM2 sequences [24]. Currently, only three MLLE-containing proteins are described:
the poly(A)-binding protein, the E3 ubiquitin ligase UBR5 and mRNA transporter Rrm4.
UBR5 is a HECT-type (homologous to the E6AP C terminus) ligase that functions in
translational regulation and microRNA-mediated gene silencing [25].

The PAM2 motif is present in various PABC1-interaction partners such as eRF3, GW182 and PAN3 functioning in various steps of posttranscriptional control such as translation, miRISC assembly and deadenylation, respectively [26]. The vast majority of proteins harbour a single PAM2 motif, only eRF3 and Tob contain two overlapping PAM2 motifs for MLLE interaction [27, 28]. Therefore, it is exceptional to find four PAM2 motifs in Upa2 and due to the potential dimerisation via its C-terminal coiled coil region Upa2 offers an extensive interaction platform for Pab1 (Fig 7).

277 Experimental evidence confirmed that the PAM2 motifs of Upa2 interact with Pab1. 278 However, it seems to be an utter paradox that these evolutionarily conserved PAM2 motifs 279 are not important for the function of Upa2 during endosomal mRNA transport. The same 280 holds true for Upa1, where the PAM2 motif is also dispensable for function [16]. A possible 281 explanation is a high level of redundancy. This is supported by the fact that in endosomal 282 mRNPs there are verified PAM2 motifs in Upa1 and Upa2 as well as additional cryptic 283 versions in Rrm4. It is conceivable that all PAM2 sequences and their variants must be 284 mutated to observe defects in mRNA transport and consequently in hyphal growth. In fact, 285 redundancy was already observed during the study of PAM2-like motifs. Only deletion of 286 both PAM2-like sequences in Upa1 resulted in loss of function [16]. Alternatively, we might 287 not be able to detect the functional significance of the PAM2 / Pab1 interaction under optimal

Jankowski, Pohlmann et al.

laboratory conditions. The interaction could be of specific importance under certain stress
conditions. Comparably, a function of the small glycine rich protein Grp1 was only observed
during hyphal growth under cell wall stress conditions [15].

291 Besides PAM2 motifs and a coiled coil region for dimerization, we identified two 292 additional functionally important regions. Firstly, we succeeded in mapping a novel N-293 terminal effector domain. Interestingly, this domain is embedded in a part of the protein that 294 is predicted to be rich in intrinsically disordered regions (IDRs; Fig EV5). In the future, we 295 need to carry out an extensive fine mapping to identify clear boundaries of this domain and 296 identify the respective interaction partner. Secondly, we discovered a C-terminal GWW motif 297 that is essential for the endosomal localisation of Upa2. Since the presence of Upa2 depends 298 on the RNA-binding capacity of Rrm4, we assume that the GWW motif does not bind 299 endosomal lipids directly. Most likely, it interacts with a protein component of endosomal 300 mRNPs (Fig 7). This assumption is supported by the fact that an evolutionarily conserved 301 GWW motif at the C-terminus of bacterial endoribonuclease RNase E interacts with a 302 peptide-binding pocket of a PNPase (exoribonuclease polynucleotide phosphorylase; 21, 22]. 303 Furthermore, GWW motifs have been implicated in intramolecular interactions of two SH3 304 domains of the NADPH oxidase component p47^{phox} [29]. Related dispersed GW motifs in the 305 posttranslational regulator GW182 mediate recruitment of CCR4-NOT deadenvlation 306 components during miRNA-mediated repression [30]. In essence, we identified at least four 307 different types of interfaces for protein/protein interactions in Upa2 supporting the hypothesis 308 that it serves as a scaffold protein.

309 The function of Upa2 during endosomal transport

In order to study the function of Upa2 *in vivo* we combined genetic with cell biological approaches. Loss of Upa2 causes the same aberrant growth phenotype and reduced Cts1 secretion as observed in *rrm*4 Δ and *upa1\Delta* strains [13, 16], suggesting that these proteins

Jankowski, Pohlmann et al.

313 function in the same pathway. This is supported by a phylogenetic analysis showing the co-314 appearance of all three proteins.

315 The bipolar hyphal growth phenotype can in part be explained by the defects in forming 316 the gradient of septin filaments at the growth pole, since septins are important during the 317 initial phase of unipolar hyphal growth [12, 14]. The formation of the septin gradient depends 318 on the endosomal transport of septin heteromers and in turn heteromer assembly depends on 319 endosomal transport of the septin encoding mRNAs [12, 14]. Thus, the most rational 320 explanation for the observed defects in hyphal growth in $upa2\Delta$ strains is the reduced 321 transport of septin mRNAs resulting in fewer septin proteins on endosomes. Since the 322 presence of the different septins on transport endosomes are interdependent [14], the reduced 323 amount might not be able to support endosomal assembly and localisation of septin proteins 324 causing the observed defects in septin gradients. The hypothesis of local translation on the 325 endosomal surface for septin assembly [12, 14] has recently been supported by the finding 326 that most heteromeric protein complexes are co-translationally assembled in eukaryotes [31].

327 Loss of Upa2 also causes a slight increase in the amount and velocity of transport 328 endosomes suggesting that the absence of Upa2 and the reduced associated mRNA cargos has 329 an influence on transport endosomes in general. However, the most profound differences were 330 recognized studying the mRNP components Rrm4 and Pab1. We observed an aberrantly 331 strong formation of Rrm4 on microtubules and reduced endosomal localisation of Pab1. 332 Hence, Upa2 appears to be crucial for the stable association of mRNPs on the surface of 333 endosomes during transport. This is consistent with important key findings of this study that 334 Upa2, like Rrm4, specifically localises to transport endosomes and that it is present an almost 335 all transport endosomes. In conjunction with the aforementioned scaffolding function, Upa2 336 fulfils the necessary criteria to function as a novel core component of endosomal mRNP 337 transport.

Jankowski, Pohlmann et al.

338 Conclusions

In recent years the identification of components of the endosomal mRNA transport machinery in *U. maydis* has advanced significantly (Fig 7). Importantly, it is the first system, where a transcriptome-wide binding landscape of the key RBP is available. Comparing bound RNAs of Rrm4 with the accessory component Grp1 revealed that Rrm4 orchestrates a tailored transport strategy for distinct sets of cargo mRNAs [15]. Here, we add the evolutionarily conserved Upa2 as an important novel piece to our jigsaw puzzle of endosomal mRNA transport.

346 Key concepts appear to be conserved throughout evolution and might also be applicable 347 to higher eukaryotes. In fungi, for example, Rrm4, Upa1 and Upa2 are conserved throughout 348 Basidiomycetes suggesting that endosomal mRNA transport is more wide-spread than 349 currently anticipated [20]. Consistently, in animal systems, endosomal components have been 350 implicated in mRNA transport during axonal growth [32, 33] and mRNAs associated with 351 Rab5-positive endosomes were described in plants [34]. More recently, endosomal mRNA 352 transport and coupled translation at late endosomes were described to be crucial for 353 mitochondrial function in polar growing axons [35]. Hence, endosome-coupled translation 354 seems to be conserved from fungi to men and is now critical to obtain insights in the 355 mechanisms of how mRNPs stably associate with endosomes [36]. Finally, discovering the 356 key RNA-binding protein Rrm4 that is linked intensively and intimately with endosomal 357 membranes fits to the new emerging concept that RNA and membrane biology are tightly 358 intertwined. Membrane-associated RBPs (memRBPs) are most likely important at all 359 intracellular membranes to orchestrate spatio-temporal expression [37]. These findings stress 360 the vital role of *U. maydis* as a model for RNA biology [4, 10].

361

16

Jankowski, Pohlmann et al.

362 Materials and methods

363 Plasmids, strains and growth conditions

364 For cloning of plasmids and GST pulldown experiments, E. coli Top10 cells (Life Technologies, Carlsbad, CA, USA) and E. coli Rosetta2 pLysS (Merck 71403) were used, 365 366 respectively. Transformation, cultivation and plasmid isolation were conducted using standard techniques. All U. maydis strains are derivatives of AB33, in which hyphal growth can be 367 368 induced [18]. Yeast-like cells were incubated in complete medium (CM) supplemented with 369 1% glucose, whereas hyphal growth was induced by changing to nitrate minimal medium 370 (NM) supplemented with 1% glucose, both at 28°C [18]. Detailed growth conditions and 371 cloning strategies for U. maydis are described elsewhere [8, 38, 39]. All plasmids were 372 verified by sequencing. Strains were generated by transforming progenitor strains with 373 linearised plasmids. Successful integration of constructs was verified by diagnostic PCR and 374 by Southern blot analysis [38]. For ectopic integration, plasmids were linearised with SspI 375 and targeted to the ip^{S} locus [40]. Wild-type strain UM521 genomic DNA was used as a 376 template for PCR amplifications of ORFs, unless otherwise stated. Yeast two-hybrid tests 377 were carried out using S. cerevisiae strain AH109 (Clontech Laboratories Inc., Mountain 378 View, CA, USA). A detailed description of all plasmids and strains is given in Appendix 379 Tables S1 to S6. Sequences are available upon request.

380 Microscopy, image processing and image analysis

Laser-based epifluorescence-microscopy was performed on a Zeiss Axio Observer.Z1 equipped with CoolSNAP HQ2 CCD (Photometrics, Tuscon, AZ, USA) and ORCA-Flash4.0 V2+ CMOS (Hamamatsu Photonics Deutschland GmbH, Geldern, Germany) cameras. For excitation we used a VS-LMS4 Laser-Merge-System (Visitron Systems, Puchheim, Germany) that combines solid state lasers for excitation of Gfp (488 nm at 50 or 100 mW) and Rfp/mCherry (561 nm at 50 or 150 mW).

17

Jankowski, Pohlmann et al.

For the quantification of unipolar hyphal growth, cells were grown in 20 ml cultures to an OD₆₀₀ of 0.5 and hyphal growth was induced. After 6 hours, more than 100 cells per experiment were imaged and analysed for growth behaviour. Cells were scored for unipolar and bipolar growth as well for formation of empty sections. At least three independent experiments were conducted. For statistical analysis, the rate of bipolarity was investigated by using unpaired two-tailed Student's t-test.

393 For analysis of signal number and velocity, we recorded videos with an exposure time of 394 150 ms and 150 frames taken. All videos and images were processed and analysed using 395 Metamorph (Version 7.7.0.0, Molecular Devices, Seattle, IL, USA). Kymographs were 396 generated using a built-in plugin and processively moving particles were counted manually. 397 The average velocity was determined by quantifying processive signals (movement > 5 μ m). 398 Data points represent means from three independent experiments (n = 3) with mean of means 399 (red line) and s.e.m. For each experiment at least 30 signals per hypha were analysed out of 400 10 hyphae per strain.

For quantification of Cdc3 fluorescence intensity line-scans were conducted in a region of 10 μ m from hyphal tips. Relative fluorescence intensities of 30 hyphal tips per strain were averaged. Data points represent means from three independent experiments (n = 3) with mean of means (red line) and s.e.m.. Colocalization studies of dynamic processes were carried out by using a two-channel imaging system (DV2, Photometrics, Tucson, AZ, USA) [16, 41].

406 **RNA live imaging, FM4-64 staining and benomyl treatment**

407 RNA imaging in living cells was conducted by using the λ N-based green-RNA method 408 described previously [12, 14]. For RNA visualization of *ubi1* and *rho3* λ N was fused to three 409 copies of enhanced Gfp and 16 copies of the boxB loop were inserted in the 3' UTR of the 410 respective mRNAs. Expression was driven either by the native *ubi1* promoter or in case of 411 *rho3* by the constitutively active promoter P_{otef}. For RNA visualization of *cdc3* and *cdc12* a

Jankowski, Pohlmann et al.

412 modified λN (λN^*) was fused to three copies of enhanced Gfp and 16 copies of the boxB loop 413 were inserted in the 3⁻ UTR of the respective mRNAs. Both constructs were under the control 414 of the constitutive active promoter P_{otef} . Three independent experiments (n = 3) were 415 conducted with at least 10 hyphae per strain. Statistical tests were performed using Graphpad 416 Prism5 (version 5.00; Graphpad Software, La Jolla, CA, USA). A detailed protocol for 417 subsequent data analysis was described elsewhere [14]. For staining of cells with FM4-64, a 1 418 ml sample of hyphal cells was labelled with 0.8 µM FM4-64 (Thermo Fisher, Waltham, MA, 419 USA). After incubation for 1 min at room temperature, the labelled cells were analysed by 420 fluorescence microscopy. For benomyl treatment, a 1 ml sample of hyphal cells was treated 421 with 20 µM benomyl (Sigma-Aldrich, Taufkirchen, Germany). After incubation for 30 min at 422 room temperature with agitation samples were analysed by microscopy.

423 Fluorimetric measurement of chitinolytic activity

424 Chitinolytic activity measurements of U. maydis cells were carried out as described elsewhere 425 [16, 19]. Briefly, U. maydis cell suspensions were grown to an OD₆₀₀ of 0.5. The culture was 426 divided in half, yeast-like growing cells were measured directly while activity of hyphae was 427 measured 6 h after induction of hyphal growth. 30 µl of the culture were mixed with 70 µl 428 0.25 μM 4-Methylumbelliferyl-β-D-N,N',N''-triacetylchitotrioside (MUC, Sigma-Aldrich, 429 Taufkirchen, Germany), a fluorogenic substrate for chitinolytic activity. After incubation for 1 430 h, the reaction was stopped by addition of 200 µl 1M Na₂CO₃, followed by detection of the 431 fluorescent product with the fluorescence spectrometer Infinite M200 (Tecan Group Ltd., 432 Männedorf, Switzerland) using an excitation and emission wavelength of 360 nm and 450 433 nm, respectively. Chitinase activity was set and reported in relation to AB33 (wt) activity. 434 Five independent biological experiments were performed with three technical replicates per 435 strain.

Jankowski, Pohlmann et al.

436 Yeast two-hybrid analysis

437 The yeast two-hybrid analyses were carried out as described elsewhere [16]. Briefly, using the 438 two-hybrid system Matchmaker 3 from Clontech, strain AH109 was co-transformed with 439 derivates of pGBKT7-DS and pGADT7-Sfi (Appendix Table S4) and cells were grown on 440 synthetic dropout (SD) plates without leucine and tryptophan at 28° C for 4 days. 441 Subsequently, colonies were patched on SD plates without leucine and tryptophan (control) or 442 on SD plates without leucine, tryptophan, histidine and adenine (selection). Plates were 443 incubated at 28°C for 3 days to test for growth under selection condition. For qualitative plate 444 assays cells were cultivated in SD without leucine and tryptophan to OD_{600} of 0.5 and 445 successively diluted with sterile water in four steps at 1:5 each. 4 µl were spotted on control 446 as well as selection plates and incubated at 28° C for 3 days. Colony growth was documented 447 with a LAS 4000 imaging system (GE Healthcare Life Sciences, Little Chalfont, UK).

448 **Protein extracts and Western blot analysis**

U. maydis hyphae were harvested 6 hours post induction (h.p.i.) by centrifugation (7546 x g, 449 450 10 minutes) and resuspended in 2 ml of either urea buffer (8 M Urea, 50 mM Tris/HCl pH8; 451 Fig EV2E and Fig EV3F, right panel) or l-arginine rich buffer (0.4 M sorbitol; 5 % glycerol; 452 50 mM Tris/HCl pH7.4; 300 mM NaCl; 1 mM EDTA; 0.5% Nonidet P-40; 0.1% SDS; 72.5 453 mM l-arginine, Fig EV3C and Fig EV3F, left panel) supplemented with protease inhibitors (1 454 tablet of complete protease inhibitor per 25 ml, Roche, Mannheim, Germany; 1 mM DTT; 0.1 455 M PMSF; 0.5 M benzamidine). Cells were lysed in a Retsch ball mill (MM400; Retsch, Haan, 456 Germany) while keeping samples constantly frozen using liquid nitrogen. 2 ml cell suspension per grinding jar with two grinding balls (d = 12 mm) were agitated for 10 minutes 457 458 at 30 Hz. Protein concentrations were measured by Bradford assay (Bio-Rad, Munich, 459 Germany) and samples were adjusted to equal amounts. For Western Blot analysis, protein 460 samples were supplemented with Laemmli buffer and heated to 60°C-80°C for 10 minutes, 461 resolved by 8% SDS-PAGE and transferred to a nitrocellulose membrane (GE Healthcare,

Jankowski, Pohlmann et al.

Munich, Germany) by semi-dry blotting. Membranes were probed with α-Gfp (Roche,
Freiburg, Germany) and α-actin (MP Biomedicals, Eschwege, Germany) antibodies. As
secondary antibody a mouse IgG HRP conjugate was used (Promega, Madison, WI, USA).
Detection was carried out by using AceGlow (VWR Peqlab, Erlangen, Germany).

466 **GST pull down experiments**

Derivatives of plasmids pGEX and pET15B (Appendix Table S5) were transformed into E. 467 468 coli Rosetta2 pLysS (Merck 71403). Overnight cultures were diluted 1:50 in a final volume of 469 50 ml. Protein expression was induced with 1mM IPTG for 4 h at 28°C. Cells were pelleted, 470 resuspended in 10 ml lysis buffer and lysed by sonication. Cell lysate was centrifuged at 471 16,000 g for 15 minutes and the supernatant was transferred to the fresh microcentrifuge 472 tubes. 50 µl glutathione beads (GE Healthcare) were transferred to a new 1.5 ml 473 microcentrifuge tube and washed 3 times with 1 ml lysis buffer (20 mM Tris-Cl, pH 7.5; 200 474 mM NaCl; 1mM EDTA, pH 8.0; 0.5 % Nonidet P-40; 1 tablet complete protease inhibitor per 475 50ml, Roche, Mannheim, Germany). For each pulldown, 1 ml of supernatant of GST-tagged 476 protein was added to the washed beads, incubated for 1 h at 4° C and subsequently washed 5 times with 1 ml lysis buffer. 1 ml supernatant containing His-tagged Upa2 variant was added 477 478 directly to the washed GST bead and incubated for 1 h at 4° C and subsequently washed 5 479 times with lysis buffer. The beads were boiled for 6 min at 99° C in 100 µl of 1x Laemmli 480 buffer. 10 µl of each GST-pulldown fraction was analysed by SDS-PAGE and Coomassie 481 blue (CBB R250) staining. 1 ml supernatant containing Upa2 variant was added directly to 482 the washed Ni-NTA (Macherey-Nagel) bead, incubated for 1 h at 4° C and subsequently 483 washed 5 times with 1 ml lysis buffer. 20 µl of each Upa2 variants were loaded on control 484 lanes in SDS PAGE as an input. Note, that the input fraction "H" shows Ni-NTA precipitated 485 Upa2, which could not be visualized before enrichment.

Jankowski, Pohlmann et al.

For Western blotting protein samples were resolved by 10% SDS-PAGE and transferred to a PVDF membrane (GE Healthcare) by semi-dry blotting. Western blot analysis was performed with α -GST (Sigma G7781), α -His (Sigma H1029). α -Rabbit IgG HRP conjugate (Promega W4011), α -mouse IgG HRP conjugate (Promega W4021) were used as secondary antibodies. Activity was detected using the AceGlow blotting detection system (VWR Peqlab, Erlangen, Germany).

492 **Phylogenetic analysis and bioinformatics**

Sequence data for U. maydis genes was retrieved from the PEDANT database 493 494 (http://pedant.gsf.de/). Accession numbers of U. maydis genes used in this study: upa2 495 (UMAG_10350), rrm4 (UMAG_10836), pab1 (UMAG_03494), upa1 (UMAG_12183), 496 rab5a (UMAG_10615) and cdc3 (UMAG_10503). Orthologs were identified using fungiDB 497 [42, 43], Ensembl Fungi [44] and NCBI blastp tool [45]. Sequences alignments were 498 performed with ClustalX (version 2.0.12) [46]. Domains were predicted using SMART [47, 499 48], conserved domain database from the NCBI (CDD) [49] and active search using 500 ScanProsite [50]. The coiled coil dimerisation domain was predicted using the Interpro 501 COILS program [51]. The phylogenetic tree is based on the NCBI taxonomy and was created 502 using phyloT online tool (phylot.biobyte.de). The lengths of the lines do not represent 503 evolutionary distance. The accession numbers for the proteins can be found in Appendix 504 Table S7).

505 Intrinsically disordered regions were predicted using the PONDR VL3-BA algorithm 506 (www.pondr.com, Molecular Kinetics, Inc., IN, USA). VL3-BA is a feedforward neural 507 network predictor generating outputs between 0 and 1 which are smoothed over a sliding 508 window of 9 amino acids. Regions with values of 0.5 or above are considered disordered and 509 are marked in red, while peptide regions with values lower than 0.5 are considered ordered 510 and are marked in blue.

22

Jankowski, Pohlmann et al.

511

512 Acknowledgements

- We acknowledge Drs. A. Brachmann, J. Béthune, K. Zarnack and lab members for discussionand reading of the manuscript. We are grateful to U. Gengenbacher for excellent technical
- assistance. The work was funded by grants from the Deutsche Forschungsgemeinschaft to MF
- 516 (FE448/5-2 DFG-FOR1334; FE448/10-1 DFG-FOR2333; DFG-CRC1208 project number
- 517 267205415 and CEPLAS EXC1028).

518

519 Author contributions

520 SJ, TP, SB and MF designed this study and analysed the data. SJ and TP contributed equally 521 to the genetic and cell biological analysis of Upa2. SB carried out the initial cell biological 522 characterisation of Upa2. KM and SZ performed RNA live imaging experiments. SKD

- 523 analysed the PAM2/MLLE interaction in vitro. MF, SJ and TP drafted and revised the
- 524 manuscript with input from all co-authors. MF and TP directed the project.
- 525

526 **Conflict of interest**

- 527 The authors declare that they have no conflict of interest.
- 528

529 References

- Martin KC, Ephrussi A (2009) mRNA localization: gene expression in the spatial
 dimension. *Cell* 136: 719-730
- 532 2. Eliscovich C, Singer RH (2017) RNP transport in cell biology: the long and winding
 533 road. *Current opinion in cell biology* 45: 38-46
- 534 3. Edelmann FT, Schlundt A, Heym RG, Jenner A, Niedner-Boblenz A, Syed MI, Paillart
- 535 JC, Stehle R, Janowski R, Sattler M, et al. (2017) Molecular architecture and dynamics of

Jankowski, Pohlmann et al.

- 536 ASH1 mRNA recognition by its mRNA-transport complex. Nat Struct Mol Biol 24: 152-
- 537 161
- 538 4. Niessing D, Jansen RP, Pohlmann T, Feldbrügge M (2018) mRNA transport in fungal top
 539 models. *Wiley interdisciplinary reviews RNA* 9: e1453
- 540 5. Mofatteh M, Bullock SL (2017) SnapShot: Subcellular mRNA localization. *Cell* 169:
 541 178.e1
- 542 6. Vollmeister E, Schipper K, Baumann S, Haag C, Pohlmann T, Stock J, Feldbrügge M
 543 (2012) Fungal development of the plant pathogen *Ustilago maydis*. *FEMS Microbiol Rev*
- **36**: 59-77
- 545 7. Haag C, Steuten B, Feldbrügge M (2015) Membrane-coupled mRNA trafficking in fungi.
 546 *Annu Rev Microbiol* 69: 265-281
- 8. Baumann S, Pohlmann T, Jungbluth M, Brachmann A, Feldbrügge M (2012) Kinesin-3
 and dynein mediate microtubule-dependent co-transport of mRNPs and endosomes. J
- 549 *Cell Sci* **125**: 2740-2752
- Schuster M, Kilaru S, Fink G, Collemare J, Roger Y, Steinberg G (2011) Kinesin-3 and
 dynein cooperate in long-range retrograde endosome motility along a non-uniform
 microtubule array. *Mol Biol Cell* 22: 3645-3657
- 10. Haag C, Pohlmann T, Feldbrugge M (2017) The ESCRT regulator Did2 maintains the
 balance between long-distance endosomal transport and endocytic trafficking. *PLoS Genet* 13: e1006734
- 556 11. Higuchi Y, Ashwin P, Roger Y, Steinberg G (2014) Early endosome motility spatially
 557 organizes polysome distribution. *J Cell Biol* 204: 343-357
- Baumann S, König J, Koepke J, Feldbrügge M (2014) Endosomal transport of septin
 mRNA and protein indicates local translation on endosomes and is required for correct
 septin filamentation. *EMBO Rep* 15: 94-102

Jankowski, Pohlmann et al.

- 561 13. König J, Baumann S, Koepke J, Pohlmann T, Zarnack K, Feldbrügge M (2009) The
- fungal RNA-binding protein Rrm4 mediates long-distance transport of *ubi1* and *rho3*mRNAs. *EMBO J* 28: 1855-1866
- 14. Zander S, Baumann S, Weidtkamp-Peters S, Feldbrügge M (2016) Endosomal assembly
- and transport of heteromeric septin complexes promote septin cytoskeleton formation. J
- 566 *Cell Sci* **129**: 2778-2792
- 567 15. Olgeiser L, Haag C, Boerner S, Ule J, Busch A, Koepke J, König J, Feldbrügge M,
 568 Zarnack K (2019) The key protein of endosomal mRNP transport Rrm4 binds
 569 translational landmark sites of cargo mRNAs. *EMBO Rep*: e46588
- 570 16. Pohlmann T, Baumann S, Haag C, Albrecht M, Feldbrügge M (2015) A FYVE zinc
 571 finger domain protein specifically links mRNA transport to endosome trafficking. *eLife*572 4: e06041
- 573 17. Becht P, König J, Feldbrügge M (2006) The RNA-binding protein Rrm4 is essential for
- 574 polarity in *Ustilago maydis* and shuttles along microtubules. *J Cell Sci* **119**: 4964-4973
- 575 18. Brachmann A, Weinzierl G, Kämper J, Kahmann R (2001) Identification of genes in the
 576 bW/bE regulatory cascade in *Ustilago maydis*. *Mol Microbiol* 42: 1047-1063
- 577 19. Koepke J, Kaffarnik F, Haag C, Zarnack K, Luscombe NM, König J, Ule J, Kellner R,
- 578 Begerow D, Feldbrügge M (2011) The RNA-binding protein Rrm4 is essential for
- 679 efficient secretion of endochitinase Cts1. *Mol Cell Proteom* **10**: M111.011213 1-15
- 580 20. Müller J, Pohlmann T, Feldbrügge M (2019) Core components of endosomal mRNA
 581 transport are evolutionarily conserved in fungi. *Fungal Genet Biol* 126: 12-16
- 582 21. Hardwick SW, Chan VS, Broadhurst RW, Luisi BF (2011) An RNA degradosome
 583 assembly in *Caulobacter crescentus*. *Nucleic Acids Res* 39: 1449-1459
- 584 22. Hardwick SW, Gubbey T, Hug I, Jenal U, Luisi BF (2012) Crystal structure of
- 585 Caulobacter crescentus polynucleotide phosphorylase reveals a mechanism of RNA
- substrate channelling and RNA degradosome assembly. *Open biology* **2**: 120028

Jankowski, Pohlmann et al.

- 587 23. Baumann S, Takeshita N, Grün N, Fischer R, Feldbrügge M (2015) Live cell imaging of
- 588 *endosomal trafficking in fungi*. In Methods in Mol Biol: Membrane trafficking, Tang BL

(ed) pp 347-363. New York: Springer

- 590 24. Kozlov G, Trempe JF, Khaleghpour K, Kahvejian A, Ekiel I, Gehring K (2001) Structure
- and function of the C-terminal PABC domain of human poly(A)-binding protein. *Proc*
- 592 Natl Acad Sci U S A **98**: 4409-4413
- 593 25. Su H, Meng S, Lu Y, Trombly MI, Chen J, Lin C, Turk A, Wang X (2011) Mammalian
 594 hyperplastic discs homolog EDD regulates miRNA-mediated gene silencing. *Mol Cell*595 43: 97-109
- 596 26. Xie J, Kozlov G, Gehring K (2014) The "tale" of poly(A) binding protein: the MLLE
 597 domain and PAM2-containing proteins. *Biochim Biophys Acta* 1839: 1062-1068
- 598 27. Kozlov G, Gehring K (2010) Molecular basis of eRF3 recognition by the MLLE domain
 599 of poly(A)-binding protein. *PLoS One* 5: e10169
- 600 28. Ezzeddine N, Chang TC, Zhu W, Yamashita A, Chen CY, Zhong Z, Yamashita Y, Zheng
- 601 D, Shyu AB (2007) Human TOB, an antiproliferative transcription factor, is a poly(A)-
- binding protein-dependent positive regulator of cytoplasmic mRNA deadenylation.
 Molecular and cellular biology 27: 7791-7801
- 604 29. Groemping Y, Lapouge K, Smerdon SJ, Rittinger K (2003) Molecular basis of 605 phosphorylation-induced activation of the NADPH oxidase. *Cell* **113**: 343-355
- 606 30. Chekulaeva M, Mathys H, Zipprich JT, Attig J, Colic M, Parker R, Filipowicz W (2011)
- miRNA repression involves GW182-mediated recruitment of CCR4-NOT through
 conserved W-containing motifs. *Nat Struct Mol Biol* 18: 1218-1226
- 609 31. Shiber A, Doring K, Friedrich U, Klann K, Merker D, Zedan M, Tippmann F, Kramer G,
- 610 Bukau B (2018) Cotranslational assembly of protein complexes in eukaryotes revealed by
- 611 ribosome profiling. *Nature* **561**: 268-272

Jankowski, Pohlmann et al.

- 612 32. Falk J, Konopacki FA, Zivraj KH, Holt CE (2014) Rab5 and Rab4 regulate axon
 613 elongation in the Xenopus visual system. *J Neurosci* 34: 373-391
- 614 33. Konopacki FA, Wong HH, Dwivedy A, Bellon A, Blower MD, Holt CE (2016) ESCRT-
- 615 II controls retinal axon growth by regulating DCC receptor levels and local protein
- 616 synthesis. *Open biology* **6**: 150218
- 617 34. Yang Y, Chou HL, Crofts AJ, Zhang L, Tian L, Washida H, Fukuda M, Kumamaru T,
- 618 Oviedo OJ, Starkenburg S, *et al.* (2018) Selective sets of mRNAs localize to extracellular
- 619 paramural bodies in the rice glup6 mutant line. *J Exp Bot* **69**: 5045-5058
- 620 35. Cioni JM, Lin JQ, Holtermann AV, Koppers M, Jakobs MAH, Azizi A, Turner-Bridger
- B, Shigeoka T, Franze K, Harris WA, *et al.* (2019) Late endosomes act as mRNA
 translation platforms and sustain mitochondria in axons. *Cell* 176: 56-72 e15
- 623 36. Rossoll W, Bassell GJ (2019) Crosstalk of local zranslation and mitochondria: powering
 624 plasticity in axons and dendrites. *Neuron* 101: 204-206
- 37. Béthune J, Jansen RP, Feldbrügge M, Zarnack K (2018) Membrane-associated RNAbinding proteins orchestrate organelle-coupled translation *Trends in cell biology* 29: 178188
- 38. Brachmann A, König J, Julius C, Feldbrügge M (2004) A reverse genetic approach for
 generating gene replacement mutants in *Ustilago maydis*. *Mol Gen Genom* 272: 216-226
- 630 39. Terfrüchte M, Joehnk B, Fajardo-Somera R, Braus G, Riquelme M, Schipper K,
- Feldbrügge M (2014) Establishing a versatile Golden Gate cloning system for genetic
 engineering in fungi. *Fungal Genet Biol* 62: 1-10
- 40. Loubradou G, Brachmann A, Feldbrügge M, Kahmann R (2001) A homologue of the
 transcriptional repressor Ssn6p antagonizes cAMP signalling in *Ustilago maydis*. *Mol Microbiol* 40: 719-730

Jankowski, Pohlmann et al.

- 636 41. Baumann S, Zander S, Weidtkamp-Peters S, Feldbrügge M (2016) Live cell imaging of
- 637 *septin dynamics in Ustilago maydis.* In Methods in Cell Biol: Septins, Gladfelter AS (ed)
- 638 pp 143-159. Elsevier Inc.
- 639 42. Stajich JE, Harris T, Brunk BP, Brestelli J, Fischer S, Harb OS, Kissinger JC, Li W,
- 640 Nayak V, Pinney DF, et al. (2012) FungiDB: an integrated functional genomics database
- 641 for fungi. *Nucleic Acids Res* **40**: D675-681
- 642 43. Basenko EY, Pulman JA, Shanmugasundram A, Harb OS, Crouch K, Starns D,
- 643 Warrenfeltz S, Aurrecoechea C, Stoeckert CJ, Jr., Kissinger JC, et al. (2018) FungiDB:
- 644 An Integrated Bioinformatic Resource for Fungi and Oomycetes. *J Fungi* **4**: e39
- 645 44. Kersey PJ, Allen JE, Allot A, Barba M, Boddu S, Bolt BJ, Carvalho-Silva D, Christensen
- M, Davis P, Grabmueller C, *et al.* (2018) Ensembl Genomes 2018: an integrated omics
 infrastructure for non-vertebrate species. *Nucleic Acids Res* 46: D802-D808
- 45. Altschul SF, Gish W, Miller W, Myers EW, Lipman DJ (1990) Basic local alignment
 search tool. *J Mol Biol* 215: 403-410
- 650 46. Larkin MA, Blackshields G, Brown NP, Chenna R, McGettigan PA, McWilliam H,
- Valentin F, Wallace IM, Wilm A, Lopez R, *et al.* (2007) Clustal W and Clustal X version
 2.0. *Bioinformatics* 23: 2947-2948
- 47. Schultz J, Milpetz F, Bork P, Ponting CP (1998) SMART, a simple modular architecture
 research tool: identification of signaling domains. *Proc Natl Acad Sci U S A* 95: 58575864
- 48. Letunic I, Bork P (2018) 20 years of the SMART protein domain annotation resource. *Nucleic Acids Res* 46: D493-D496
- 49. Marchler-Bauer A, Bo Y, Han L, He J, Lanczycki CJ, Lu S, Chitsaz F, Derbyshire MK,
- 659 Geer RC, Gonzales NR, et al. (2017) CDD/SPARCLE: functional classification of
- 660 proteins via subfamily domain architectures. *Nucleic Acids Res* **45**: D200-D203

Jankowski, Pohlmann et al.

- 661 50. de Castro E, Sigrist CJ, Gattiker A, Bulliard V, Langendijk-Genevaux PS, Gasteiger E,
- Bairoch A, Hulo N (2006) ScanProsite: detection of PROSITE signature matches and
- 663 ProRule-associated functional and structural residues in proteins. *Nucleic Acids Res* 34:
- 664 W362-5
- 51. Lupas A, Van Dyke M, Stock J (1991) Predicting coiled coils from protein sequences.
- *Science* **252**: 1162-1164
- 52. Steinberg G, Fuchs U (2004) The role of microtubules in cellular organization and
 endocytosis in the plant pathogen *Ustilago maydis*. *J Microsc* 214: 114-123

669

Jankowski, Pohlmann et al.

670 Figures 1-7 and Figure legends

671 Figure 1. Upa2 contains multiple PAM2 motifs for interaction with Pab1.

672 (A) Schematic representation of the MLLE domain-containing proteins Rrm4 and Pab1 as 673 well as the PAM2 motif-containing proteins Upa1 and Upa2 drawn to scale (bar, 200 amino 674 acids; green, RRM domain; blue, MLLE domain; orange, PAM2 motif; dark blue, PAM2-like 675 motif; dark grey, Ankyrin repeats; light blue, FYVE domain; lilac, RING domain; yellow, 676 coiled coil region) (B) Comparison of PAM2 sequences found in Upa2 (accession number 677 UMAG 10350) with those of human proteins such as PAIP1 (accession number 678 NP 006442.2), PAIP2 (accession number CAG38520.1), eRF3B (accession number 679 CAB91089.1) and ATX2 (accession number NP_002964.3). (C) Two-hybrid analysis with 680 schematic representation of protein variants tested on the left. Yeast cultures were serially 681 diluted 1:5 (decreasing colony forming units, cfu) and spotted on respective growth plates 682 controlling transformation and assaying reporter gene expression (see Materials and 683 methods). (**D**) GST co-purification experiments with components expressed in *E. coli*: MLLE 684 domain of Pab1 fused to GST and N-terminal His₆-tagged versions of Upa2 (amino acids 685 834–1216; orange rectangles indicate PAM2 motif 1, 2 and 3; black rectangles mark 686 mutations; 43 kDa). Interaction studies were performed with the soluble fraction of protein 687 extracts from E. coli to demonstrate specific binding. After GST affinity chromatography proteins were eluted (lanes marked with "E"; G, input of GST-MLLE^{Pab1} and H, Ni-NTA 688 689 precipitated His₆-Upa2). Note that the Upa2 variants were enriched in the eluate due to the pull down by MLLE^{Pab1}. (E) Two-hybrid analysis of the coiled coil region of Upa2 (amino 690 691 acids 1712-2121) fused to binding domain (BD) and activation domain (AD) of the Gal4 692 transcription factor (design as in C).

Jankowski, Pohlmann et al.

693

694 Figure 2. Loss of Upa2 causes defects in hyphal growth.

695 (A) Growth of AB33 derivatives in the hyphal form (6 h.p.i.; growth direction is marked by 696 arrows; n, nucleus; asterisks, basal septa). (B) Quantification of hyphal growth (6 h.p.i): 697 unipolarity, bipolarity and septum formation were quantified (error bars, s.e.m.; n = 3698 independent experiments, for each experiment >100 hyphae were counted per strain; note that 699 septum formation is given relative to the values of unipolar or bipolar hyphae set to 100%). 700 For statistical analysis, the percentage of bipolarity was investigated by using unpaired two-701 tailed Student's t-test. Three independent experiments (n = 3) were conducted with at least 702 100 hyphae per strain. (C) Schematic representation of orthologues of Rrm4, Upa2 and Upa1 703 in different basidiomycetes. The phylogenetic tree was generated using the phyloT tool using 704 the NCBI taxonomy (no evolutionary distances): U.m.: Ustilago maydis, U.h.: Ustilago 705 hordei; U.b.: Ustilago bromivora; S.r.: Sporisorium reilianum; S.sc.: Sporisorium 706 scitamineum, M.a.: Moesziomyces antarcticus, M.p.: Melanopsichium pennsylvanicum, T.t.: 707 Thecaphora thlaspeos; M.g.: Malassezia globosa; C.n.: Cryptococcus neoforman var 708 neoformanss; A.o.: Armillaria ostovae; C.c.: Coprinopsis cinerea; P.s.: Punctularia 709 strigosozonata; S.i.: Serendipita indica; T.v.: Trametes versicolor; P.c.: Phanerochaete 710 carnosa. * Bioinformatic tools predict weak RRM domains and a non-functional MLLE 711 domain in C.n. Rrm4. ** A.o. Upa1 contains a predicted transmembrane domain instead of a 712 RING domain; *** S.i. Upa1 was manually assembled from two consecutive ORFs. 713 Accession numbers are listed in Appendix Table S7.

Jankowski, Pohlmann et al.

714

715 Figure 3. Bidirectional movement of Upa2 on Rrm4-positive endosomes.

716 (A) Micrographs (inverted fluorescence image; size bar, 10 µm) and corresponding 717 kymographs of AB33 hyphae (6 h.p.i.) expressing Upa2-Gfp, Rrm4-Gfp or Pab1-Gfp (arrow 718 length on the left and bottom indicate time and distance, respectively). Bidirectional 719 movement is visible as diagonal lines (yellow arrowheads; n, nucleus; Video EV1). After 720 addition of the microtubule inhibitor benomyl static signals are seen as vertical lines (red 721 arrowheads; Video EV1). (B) Processive signals per 10 µm of hyphal length (data points 722 representing mean from n = 3 independent experiments, with mean of means, red line, and 723 s.e.m.; unpaired two-tailed Student's t-test, for each experiment at least 10 hyphae were 724 analysed per strain). (C) Velocity of fluorescent signals (velocity of tracks with $> 5 \mu m$ 725 processive movement; data points representing means from n = 3 independent experiments, 726 with mean of means, red line, and s.e.m.; unpaired two-tailed Student's t-test; for each 727 experiment at least 30 signals per hypha were analysed out of 10 hyphae per strain). (\mathbf{D}) 728 Kymographs of AB33 hyphae (6 h.p.i.) expressing pairs of red and green fluorescent proteins 729 as indicated. Fluorescence signals were detected simultaneously using dual-view technology 730 (arrow length as in A). Processive co-localising signals are marked by yellow arrowheads. 731 Areas of static signals are indicated by red asterisks (Video EV2). (E) Percentage of 732 processive signals exhibiting co-localisation for strains shown in D. Note, that due to the 733 weaker red fluorescence only clearly detectable red fluorescent signals were analysed for co-734 localisation with processive green fluorescent signals(data points represent means set to 100% 735 from n = 3 independent experiments, with mean of means, red line, and s.e.m.; unpaired two-736 tailed Student's t-test; for each experiment 6 hyphae were analysed per strain).

Jankowski, Pohlmann et al.

737

738 Figure 4. Endosomal localisation of Upa2 is mRNA-dependent.

739 (A) Micrographs (inverted fluorescence image: size bar, 10 µm) and corresponding 740 kymographs of AB33 hyphae (6 h.p.i.). Genetic background as indicated above (arrow length 741 on the left and bottom indicate time and distance, respectively). Bidirectional movement is 742 visible as diagonal lines (yellow arrowheads; Videos EV3-EV5). (B) Processive signals per 743 10 μ m of hyphal length (data points representing means from n = 3 independent experiments, 744 with mean of means, red line, and s.e.m.; unpaired two-tailed Student's t-test, for each 745 experiment at least 10 hyphae were analysed per strain). (C) Kymographs of AB33 hyphae (6) 746 h.p.i.) expressing pairs of red and green fluorescent proteins as indicated. Fluorescence 747 signals were detected simultaneously using dual-view technology (arrow length as in A). 748 Processive co-localising signals are marked by yellow arrowheads (Videos EV6-EV7). (**D**) 749 Processive signals per 10 μ m of hyphal length (data points representing means from n = 3 750 independent experiments; with mean of means, red line, and s.e.m.; unpaired two-tailed 751 Student's t-test, for each experiment at least 10 hyphae were analysed per strain).

Jankowski, Pohlmann et al.

752

Figure 5. Upa2 carries a functional important effector domain at the N-terminus and a C-terminal GWW motif for endosomal localisation.

755 (A) Growth of AB33 derivatives in the hyphal form (6 h.p.i.; growth direction is marked by 756 arrows; asterisks, basal septa; n, nucleus; size bar 10 µm). (B) Quantification of hyphal 757 growth (6 h.p.i): unipolarity, bipolarity and septum formation were quantified (error bars, 758 s.e.m.; n = 3 independent experiments, for each experiment >100 hyphae were counted per 759 strain; note that septum formation is given relative to the values of unipolar or bipolar hyphae 760 set to 100%). (C) Schematic representation of N-terminal truncations of Upa2 (orange, PAM2 761 motif; light flow red, effector domain; yellow, dimerization domain; red, GWW; black, 762 mutation in GWW). (D) Quantification of hyphal growth of N-terminally truncated Upa2 763 mutants (6 h.p.i): unipolarity, bipolarity and septum formation were quantified (error bars, 764 s.e.m.; n = 3 independent experiments, for each experiment >100 hyphae were counted per 765 strain: note that septum formation is given relative to the values of unipolar or bipolar hyphae 766 set to 100%). For statistical analysis, the percentage of bipolarity was investigated by using 767 unpaired two-tailed Student's t-test. Three independent experiments (n = 3) were conducted 768 with at least 100 hyphae per strain. (E) (F) Kymographs of AB33 hyphae (6 h.p.i.); genetic 769 background as indicated (arrow length on the left and bottom indicate time and distance, 770 respectively). Bidirectional movement is visible as diagonal lines (yellow arrowheads). (G) 771 Comparison of the C-terminal amino acid sequence of Upa2 in U. maydis and related fungal 772 species. Accession numbers can be found in Appendix Table S7. (H) Growth of AB33 773 derivatives in the hyphal form (6 h.p.i.; growth direction is marked by arrows; asterisks, basal 774 septa; size bar, 10 µm) and corresponding kymographs of AB33 hyphae (6 h.p.i.). Genetic 775 background as indicated in left bottom panel (arrow length on the left and bottom indicate

Jankowski, Pohlmann et al.

- time and distance, respectively). Bidirectional movement is visible as diagonal lines (yellow
- arrowheads; Video EV8).

Jankowski, Pohlmann et al.

778

779 Figure 6. Loss of Upa2 causes defects in the formation of endosomal mRNPs.

780 (A) Micrographs of hyphal tips (inverted fluorescence image; size bar, 10 µm) and 781 corresponding kymographs of AB33 hyphae (6 h.p.i.). Genetic background as indicated above 782 (arrow length on the left and bottom indicate time and distance, respectively). Bidirectional 783 movement is visible as diagonal lines (yellow arrowheads; size bar, 10 µm; Videos EV9-12). 784 (B) Processive signals per 10 μ m of hyphal length (data points representing means from n = 3 785 independent experiments, with mean of means, red line, and s.e.m.; unpaired two-tailed 786 Student's t-test. For each experiment at least 10 hyphae per strain were analysed. (C) Velocity 787 of fluorescent signals (velocity of tracks with $> 5 \mu m$ processive movement; data points 788 representing means from n = 3 independent experiments; with mean of means, red line, and 789 s.e.m.; unpaired two-tailed Student's t-test, for each experiment at least 30 signals per hypha 790 were analysed out of 10 hyphae per strain). (D) Micrographs of hyphae and corresponding 791 kymographs of AB33 derivatives (8 h.p.i.). Genetic background as indicated above (arrow 792 length on the left and bottom indicate time and distance, respectively). Bidirectional 793 movement of mRNA is visible as diagonal lines (vellow arrowheads; size bar, 10 µm; Video 794 EV13). (E) Number of particles per 100 μ m hypha (data points representing means from n = 3 795 independent experiments, with mean of means, red line, and s.e.m.; unpaired two-tailed 796 Student's t-test, for each experiment at least 7 hyphae were analysed per strain). (F) Range of 797 movement of motile mRNAs (red line, median; n = 3 independent experiments; unpaired 798 Student's t-test). (G) Micrographs of hyphal tips (inverted fluorescence image; size bar, 10 799 µm) and corresponding kymographs of AB33 hyphae (6 h.p.i.). Genetic background as 800 indicated above (arrow length on the left and bottom indicate time and distance, respectively). 801 Bidirectional movement is visible as diagonal lines (vellow arrowheads; size bar, 10µm; 802 Video EV14). (H) Heat maps of hyphal tips (6 h.p.i.) of AB33 derivatives expressing Cdc3-

Jankowski, Pohlmann et al.

803	Gfp comparing wild type (top panel) with $rrm4\Delta$ and $upa2\Delta$ strains (middle, bottom panel),
804	indicating relative fluorescence intensity differences (maximum projection of z-stacks; size
805	bar, 10 μ m; red/yellow to green/blue, high to low intensities). (I) Relative fluorescence
806	intensity (RFU), first 10 μ m from hyphal tip (data points representing means from n = 3
807	independent experiments, with mean of means, red line, and s.e.m.; unpaired two-tailed
808	Student's t-test, for each experiment at least 10 hyphae were analysed per strain).

Jankowski, Pohlmann et al.

809

810 Figure 7. Model depicting Upa2 as novel core component of endosomal mRNP 811 transport.

812 (A) Schematic drawing of infectious hypha (red, septin filaments with gradient; green, 813 microtubules; grey circles with golden edge, transport endosomes with mRNPs and molecular 814 motors attached; boxed region is enlarged in B). (B) Simplified view of known mRNP 815 components at the cytoplasmic surface of transport endosome and a proposed interplay. Upa2 816 harbours at least four different protein/protein interfaces: PAM2 motifs (orange), effector 817 domain (light red), dimerisation domain (yellow), GWW motif (dark red). MLLE domains of 818 Pab1 and Rrm4 are given in purple. Additional symbols: 5' cap, blue circle; mRNA as blue 819 line with ORF (thick line); translating ribosome (grey) with nascent chain (black). Additional 820 mRNP components that are predicted to interact with Upa2 are given as grey circles labelled 821 X and Y (for further details, see text).

Jankowski, Pohlmann et al.

822 Expanded View Figure Legends

823

824 Figure EV1. PAM2 motifs of Upa2 do not interact with MLLE domains of Rrm4.

825 (A-B) Two-hybrid analysis with schematic representation of protein variants tested on the left (Colour scheme as in Fig 1A, C). Yeast cultures were serially diluted 1:5 (decreasing colony 826 827 forming units, cfu) and spotted on respective growth plates controlling transformation and 828 assaying reporter gene expression (see Materials and methods). (C) GST co-purification 829 experiments with components expressed in E. coli: N-terminal His6-tagged versions of Upa2⁸³⁴⁻¹²¹⁶, Upa2^{834-1216_mP23}, and Upa2^{834-1216_mP234} (amino acids 834–1216; mutation in the 830 831 PAM2 motifs number 2 and 3 as well as 2, 3 and 4, respectively) were tested for binding to the MLLE domain of Rrm4 (GST fusion to Rrm4720-792 containing two MLLE domains). Lane 832 833 "H" shows Ni-NTA precipitated His₆-Upa2, lane "G" shows input of GST- Rrm4⁷²⁰⁻⁷⁹²). After 834 GST affinity chromatography proteins were eluted (lanes marked with "E"). Interaction 835 studies were performed with the soluble fraction of protein extracts from E. coli to 836 demonstrate specific binding. (D) GST co-purification experiments as shown in B. The absence of Upa2⁸³⁴⁻¹²¹⁶ interaction with the MLLE domains of Rrm4 was demonstrated in 837 838 more sensitive Western blot experiments (used antibodies are given on the right). The three 839 lanes on the right show all Upa2 versions after Ni-NTA precipitation.

Jankowski, Pohlmann et al.

840

841 Figure EV2. Loss of Upa2 causes defects in secretion of chitinase Cts1.

842 (A) Growth of yeast cells of indicated strains in liquid culture. (B) DIC images of yeast cells 843 (size bar, 10 µm). (C) Quantification of hyphal growth (6 h.p.i): unipolarity, bipolarity and 844 septum formation were quantified (error bars, s.e.m.; n = 3 independent experiments, for each 845 experiment >100 hyphae were counted per strain; note that septum formation is given relative 846 to the values of unipolar or bipolar hyphae set to 100%). For statistical analysis, the 847 percentage of bipolarity was investigated by using unpaired two-tailed Student's t-test. Three 848 independent experiments (n = 3) were conducted with at least 10 hyphae per strain. (D) 849 Relative chitinase activity mainly detecting chitinase Cts1 [16] in yeast (left) or hyphal form 850 (right, error bars, s.e.m.; n = 5 independent experiments). For statistical analysis, the relative 851 chitinolytic activity was tested by using unpaired two-tailed Student's t-test. Five independent 852 experiments (n = 5) were conducted. (E) Western blot analysis demonstrating equal amounts 853 of Upa2-Gfp versions using aGfp antibody (top panel). Expected molecular weight: Upa2-854 Gfp, 259 kDa; Pab1-Gfp, 98 kDa; Upa1-Gfp, 166 kDa. Note, that the molecular weight of 855 Upal-Gfp appeared larger in gel electrophoresis. Actin served as a loading control using 856 α -actin antibody (bottom panel; expected size for actin, 42 kDa). Asterisks in α Gfp panels 857 mark putative degradation products of Gfp-tagged Upa2.

Jankowski, Pohlmann et al.

858

859 Figure EV3. The GWW motif of Upa2 is essential for correct hyphal growth.

860 (A) Kymographs of AB33 hyphae (6 h.p.i.) expressing versions of Upa2-Gfp with mutations in PAM2 motif as indicated (arrow length on the left and bottom indicate time and distance, 861 862 respectively). Bidirectional movement is visible as diagonal lines (yellow arrowheads). (B) 863 Quantification of hyphal growth (6 h.p.i): unipolarity, bipolarity and septum formation were 864 quantified (error bars, s.e.m.; n = 3 independent experiments, for each experiment >100 865 hyphae were counted per strain; note that septum formation is given relative to the values of 866 unipolar or bipolar hyphae set to 100%). For statistical analysis, the percentage of bipolarity 867 was investigated by using unpaired two-tailed Student's t-test. (C) Western blot analysis 868 comparing protein amounts of functional and non-functional N-terminal truncations of Upa2-Gfp (Upa2³³⁹⁻²¹²¹-Gfp, 224 kDa; Upa2³⁹⁹⁻²¹²¹-Gfp, 217 kD, respectively) using αGfp antibody 869 870 (top panel). Note, that the molecular weight appeared smaller in gel electrophoresis, most 871 likely due to the use of a l-arginine buffer (see Materials and Methods). Actin served as a 872 loading control using a ctin antibody (bottom panel; expected size for actin, 42 kDa). 873 Asterisks in α Gfp panels mark putative degradation products of Gfp-tagged Upa2. (**D**) 874 Processive signals per 10 μ m of hyphal length (data points representing means from n = 3 875 independent experiments, with mean of means, red line, and s.e.m.; unpaired two-tailed 876 Student's t-test. for each experiment at least 10 hyphae were analysed per strain). (E) Velocity 877 of fluorescent signals (velocity of tracks with $> 5 \mu m$ processive movement; data points 878 representing means from n = 3 independent experiments; with mean of means, red line, and 879 s.e.m.; unpaired two-tailed Student's t-test, for each experiment at least 30 signals per hypha 880 were analysed out of 10 hyphae per strain). (F) Western Blot analysis comparing Upa2-Gfp versions with mutations in the C-terminal GWW motif (Upa2-Gfp, 259 kDa; Upa2^{mGWW}-Gfp, 881 258 kDa; Upa2¹⁹⁵⁸⁻²¹²¹-Gfp, 46 kDa; Upa2^{1958-2121mGWW}-Gfp, 46 kDa). Note that due to the 882

Jankowski, Pohlmann et al.

883	change of two tryptophans to alanine, the running behaviour of Upa2 ^{1958-2121mGWW} -Gfp was
884	different from Upa2 ¹⁹⁵⁸⁻²¹²¹ -Gfp. Actin served as a loading control using α actin antibody
885	(bottom panel; expected size for actin, 42 kDa). Asterisks in α Gfp panels mark putative
886	degradation products of Gfp-tagged Upa2. (G) Quantification of hyphal growth (6 h.p.i):
887	unipolarity, bipolarity and septum formation were quantified (error bars, s.e.m.; $n = 3$
888	independent experiments, for each experiment >100 hyphae were counted per strain; note that
889	septum formation is given relative to the values of unipolar or bipolar hyphae set to 100%).
890	For statistical analysis, the percentage of bipolarity was investigated by using unpaired two-
891	tailed Student's t-test.

Jankowski, Pohlmann et al.

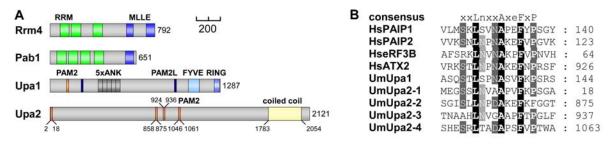
892 Figure EV4. Loss of Upa2 causes aberrant bundle-like accumulation of Rrm4-Gfp.

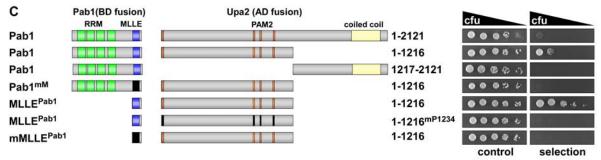
893 (A) Micrographs (inverted fluorescence image; size bar, 10 µm of AB33 hyphae (6 h.p.i.) 894 expressing Rrm4-Gfp (green arrowheads indicate bundle-like accumulation of Rrm4-Gfp). 895 (B) Micrographs (inverted fluorescence image; size bar, 10 µm) of AB33 hyphae (6 h.p.i.) 896 expressing Tub1-Gfp (ectopic expression of Tub1 fused N-terminally with Gfp) [52] or 897 Rrm4-Gfp (green arrowheads indicate bundle-like accumulation of Rrm4-Gfp). Hyphae on 898 the right were treated with the microtubule inhibitor benomyl. (C) Quantification of bundle 899 structures in strains expressing Gfp-Tub1 or Rrm4-Gfp with and without treatment of 900 microtubule inhibitor benomyl (data points representing percentages from n = 3 independent 901 experiments, with mean of means, red line; for each experiment at least 10 hyphae were 902 analysed per strain). (D) (A) Schematic representation of the $\lambda N / \lambda N^*$ RNA live imaging 903 system (P_{otef}, constitutively active promoter; P_{crg} arabinose-induced promoter) T_{nos} . 904 heterologous transcriptional terminator; ubi1, ubiquitin fusion protein; rho3, small GTPase; 905 cdc3 and cdc12, septins). All tested target genes carried 16 copies of the boxB hairpin in their 906 3' UTR. λN^*Gfp^3 is recruited to mRNAs containing the λN -binding sites designated boxB 907 [14]. (E) Velocity of fluorescent signals of analysed mRNAs (velocity of tracks with $> 3 \mu m$ 908 processive movement; data points representing means from n = 3 independent experiments, 909 with mean of means, red line, and s.e.m.; unpaired two-tailed Student's t-test; for each 910 experiment more than seven hyphae were analysed per strain). Merged datasets of all values 911 are shown.

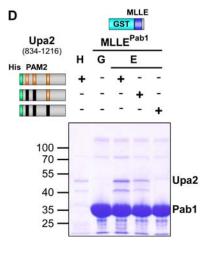
Jankowski, Pohlmann et al.

912 Figure EV5. Upa2 has extensive intrinsically disordered regions.

913 Analysis of intrinsically disordered regions using the PONDR algorithm VL3-BA. Amino 914 acids are given prediction values between 0 and 1. Regions with values of 0.5 or above are 915 considered disordered and are marked red, while peptide regions with values lower than 0.5 916 are considered ordered and are marked blue. The graphical output for the prediction is 917 depicted in relation to the protein, shown below the graph. The size of the protein models is 918 adjusted to the graph size. Extensive regions of Upa2 (>80%) are predicted to be disordered. 919 Additionally, further known components of endosomal mRNA-transport, Rrm4, Upa1 and 920 Pab1, show significant disordered stretches. Gapdh of U. maydis is shown as a structured 921 protein in comparison.







Е

	BD-fusion
1721-2121	
vector contr	rol
1721-2121	

AD-fusion		
	1721-2121	
	1721-2121	
	vector control	

fu	cfu
● ● # ×	🔍 🕘 🤴 😫 👋
0 🛛 🖓 🎌	
control	selection

ci

•

0

